ACS APPLIED MATERIALS & INTERFACES

Research Article

www.acsami.org

Bipolar Host with Multielectron Transport Benzimidazole Units for Low Operating Voltage and High Power Efficiency Solution-Processed Phosphorescent OLEDs

Xinxin Ban,[†] Wei Jiang,*[,†] Kaiyong Sun,[†] Xinyu Xie,[†] Lang Peng,[†] Hongshuang Dong,[†] Yueming Sun,*[,†] Bin Huang,[†] Lian Duan,*[,‡] and Yong Qiu[‡]

[†]School of Chemistry and Chemical Engineering, Southeast University, Nanjing, Jiangsu 211189, P. R. China

[‡]Department of Chemistry, Tsinghua University, Beijing 100084, P. R. China

ABSTRACT: Two soluble bipolar host materials (mCP-BPBI and CP-QPBI), comprising different proportions of hole-transporting carbazole and electron-transporting benzimidazole, were synthesized. Their thermal, physical, and electrochemical properties were characterized. The designated bulky star-shaped structures efficiently suppress the direct intramolecular interaction between the donor and acceptor subunits to give high triplet energies. Through computational studies, varying the ratio of hole- and electron-transporting moieties could significantly change the carrier injection/transporting abilities and charge balance properties of the host materials. Indeed, CP-QPBI with more benzimidazole units shows extremely enhanced current density at the same voltage when compared to mCP-BPBI. The operating voltage of solution-processed phosphorescent light-emitting diodes with CP-QPBI as host were dramatically reduced by ~3 V compared with the similar devices of mCP-BPBI. At the same time, the power efficiencies were improved for 2−2.5 times at the corresponding voltage. Importantly, both blue and green devices maintain their high efficiencies even at brightness up to 1000 cd m^{-2}, which clearly demonstrates that the new strategy applied to improve electron-transporting ability and charge-balance property of the solution-processable host material by tuning the ratio of donor and acceptor unit is profitable.

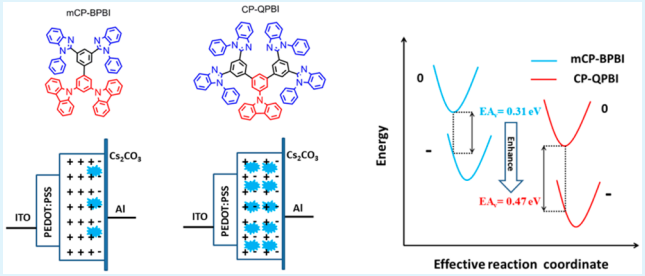

KEYWORDS: *bipolar host, reorganization energy, solution-process, low operating voltage, high power efficiency, OLEDs*

1. INTRODUCTION

Solution-processed organic light-emitting diodes (OLEDs) are being investigated widely for their potential application within flexible displays and large-area solid-state lighting.[1−6] Even though solution process is an ideal choice for obtaining low-cost and high-productivity devices, the performance of the solution-processed device is still one of the primary research concerns.[7−10] To achieve high efficiency, OLEDs should possess both high internal quantum efficiency and low operation voltage at the same time. Currently, the internal quantum efficiency has reached almost 100% by using heavy metal-centered phosphors, as they have the ability to harvest both singlet and triplet electrogenerated excitons for emission.[11,12] Therefore, the key issue to realize high power efficiency is the reduction in operating voltage.[13]

In the past few years, by using cross-link hole-transporting or alcohol-soluble electron-injection materials to optimize device architecture, the luminance efficiency of solution-processed OLEDs has been improved considerably.[14−17] Despite recent improvements, the operating voltage of solution-processed devices is still inferior to their respective vacuum-deposited counterparts for which a complex multilayer device architecture can be realized for reducing the respective injection barriers.[13,18] However, sequential deposition of hole- or electron-transport layers (ETLs) will be inherently difficult for the solution-processing technique, because the solvent used to deposit the subsequent layer tends to dissolve or swell the underlying layer.[19] As a consequence, solution-processed OLEDs are requiring high internal fields and thus high operating voltages to overcome barriers and drive the carried electrons into the emission region.

For more reduction of the operating voltages of solution-processed phosphorescent device, a particular challenge will be the development of suitable host materials.[20,21] Su and Kido et al. have reported blue and green phosphorescent OLEDs (PHOLEDs) with extremely low operating voltages through host with low ΔE_{ST} (singlet−triplet exchange energy) in the past few years.[22,23] However, solution-processable hosts with small ΔE_{ST} are rare in scientific literature as large molecular configurations are required to enhance the film-forming property. Fortunately, electron transport (ET)-type host materials with low electron-injection barriers and high electron

Received: January 17, 2015
Accepted: March 18, 2015
Published: March 18, 2015

DOI: 10.1021/acsami.5b00510
ACS Appl. Mater. Interfaces 2015, 7, 7303−7314

mobility are promising candidates for reducing the operating voltage and improving the device performance.[24] For example, Debeaux and Johannes et al. utilized electron-transporting polymers based on phenylbenzo[*d*]imidazole (PBI) moieties to obtain low operating voltages solution-processed PHOLEDs.[25] Nevertheless, the devices based on mixed unipolar hosts have a short operational lifetime and suffer from phase separation.[26,27]

Recently, great experimental efforts have focused on designing host material with bipolar property,[28] since the incorporation of hole- and electron-transporting units provide more balanced charge transporting in the emission layer, which potentially simplifies the device structure.[29] Nevertheless, challenge remains. For designing universal host materials used for solution process, an essential compromise between the molecular weight and triplet energy is inevitable, since the former requires a large conjugated group, whereas a smaller conjugated length benefits the latter. Ge and Kakimoto et al., using triphenylamine as core, designed a series of bipolar hosts for solution-process; due to their low triplet energy, the luminous efficiency of green PHOLEDs is only 4.3 cd A^{-1}. Although the triplet energy can be increased by incorporation of the methyl groups, such design configuration tragically makes the turn-on voltage as high as 13.5 V, which extremely decreases the power efficiency of the devices.[7] Commonly, carbazole is used as the repeating unit due to its sufficiently high T_1 energy and good hole-transporting ability.[30,31] In addition, by incorporating repeating units at the 3 and 6 positions of phenylcarbazole (CP), the molecular size and thermal stability will significantly increase to form high-quality films by solution process, while maintaining the high triplet energy.[32] However, this approach may result in an unbalanced charge injection into the emission layer (EML) and then a decrease in the device performance.[33,34] In comparison to the intensive efforts made on designing unipolar large molecular dendrimer by carbazole unit, the development of bipolar host materials with multi-electron transporting moieties used for solution process has not progressed greatly. To deal with the relatively weak electron mobility, which is induced by the solvent impurities and diffused oxygen-generated electron traps, the rational design of electron-transporting moieties of the bipolar host is one of the main factors to enhance the device power efficiency.[24,35−37]

In this work, we designed, synthesized, and characterized two new bipolar host materials, namely, mCP-bisPBI and CP-quadriPBI, by incorporating electron-donor carbazole with multielectron-acceptor benzimidazole units linked through the phenyl core by a metasubstitution. In this molecular design, the electronic coupling between the electron-donating and electron-withdrawing moieties can be effectively blocked to retain a reasonably high E_T. Meanwhile, the influence of the increased benzimidazole moieties on the charge-injection and charge-transporting properties of the bipolar host was investigated by density functional theory (DFT) calculations and single-carrier devices. We found that the increase of the electron-transporting units can effectively enhance both the electron injection and transporting abilities of the host, which would ensure the charge balance in the solution-processed emission layer and reduce the resistance of the device, leading to low operation voltage and high power efficiency. Indeed, a CP-QPBI-based solution-processed green PHOLED doped with tris(2-(4-tolyl)henylpyridine)iridium exhibited a very low turn-on voltage (2.9 V) and high electroluminescence efficiencies of 46.7 cd A^{-1} and 27.8 lm W^{-1}. Comparing to the device with mCP-BPBI as host, the operating voltage at 100 cd m^{-2} and driving voltage at 1000 cd m^{-2} of CP-QPBI-based device are decreased by 3.4 and 4.8 V, respectively. Meanwhile, the power efficiency is almost doubled when using CP-QPBI as host, and a similar phenomenon was also found in FIrpic-based blue PHOLEDs. These results demonstrate that using bipolar host with multielectron transport moieties will be the perfect alternatives for solution-processed PHOLEDs compared to the traditional unipolar carbazole-based dendrimers or poly(9-vinylcarbazole) (PVK) polymer.

2. EXPERIMENTAL SECTION

General Information. All reactants and solvents used for the synthesis of the compounds, unless otherwise stated, were purchased from Aldrich and Acros and used without further purification. The UV−vis absorption spectra of the compounds were recorded on SHIMADZU UV-2450. The photoluminescence (PL) emission spectra were measured by HORIBA FLUOROMAX-4, and liquid nitrogen was placed into the optical Dewar flask for low-temperature (77 K) photophysical measurements. ^{1}H NMR and ^{13}C-HMR spectra were recorded on a BRUKER AMX 300 or 500 MHz instrument relative to $Si(CH_3)_4$ as internal standard. Molecular masses were measured by a BRUKER DALTONICS matrix-assisted laser desorption-ionization time-of-flight mass spectrometry (MALDI-TOF-MS). Elemental analysis was determined by an Elementar Vario EL CHN elemlental analyzer. Thermogravimetric analysis (TGA) and differential scanning calorimetry (DSC) curves were recorded with a Netzsch simultaneous thermal analyzer (STA) system (STA 409PC) and DSC 2910 modulated calorimeter under a dry nitrogen gas flow at a heating rate of 10 °C min^{-1}. Cyclic voltammetry (CV) was performed on a CHI750C voltammetric analyzer in a typical three-electrode cell with a platinum plate working electrode, a silver wire reference electrode, and a platinum wire counter electrode. All electrochemical experiments were performed after bubbling with a constant nitrogen flow for 15 min at room temperature in CH_2Cl_2 or *N*,*N*-dimethylformamide (DMF). AFM (Seiko Instruments, SPA-400) was used to measure the film surface morphology.

Quantum Chemical Calculations. DFT simulations were performed for optimizing the molecular structures in cationic, anionic, and neutral states of mCP-BPBI or CP-QPBI. The triplet states in vacuum and the values of k^+ and k^- were all calculated without any assistance of experimental data by B3LYP at the level of 6-31G(d). Gauss-view 5.0 was used to visualize the spin-density distributions of the compounds, and all calculations were performed using the Gaussian 09 program.

OLED Fabrication and Performance Measurements. In general, indium−tin oxide (ITO)-coated glass substrates with a sheet resistance of 30 Ω/cm^{-1} were precleaned with deionized water and treated in an ultraviolet-ozone chamber. The PEDOT:PSS aqueous solution was pin-coated onto the ITO substrate as anode buffer layer and baked for 10 min at 200 °C. Then the emission layer of mCP-BPBI or CP-QPBI doped with FIrpic or $Ir(mppy)_3$ was spin-coated onto the PEDOT:PSS layer to give uniform thin films. After that, the 2,2′,2″-(1,3,5-benzinetriyl)-tris(1-phenyl-1*H*-benzimidazole) (TPBI) was evaporated as electron-transporting layer, whereas Cs_2CO_3/Al was used as the metal cathode. For hole-only devices, the host layer was spin-cast on PEDOT-modified ITO glass, and then Al electrode was deposited. For preparing electron-only devices, the host layer was directly spin-coated on ITO glass, and then Cs_2CO_3/Al electrodes were thermally deposited. The current density−voltage−brightness (*J*−*V*−*L*) characteristics of the devices and electroluminescent spectra were characterized with Keithley 4200 semiconductor characterization system and Photo Research PR705 Spectrophotometer, respectively.

Materials. The synthetic procedures for mCP-BPBI and CP-QPBI were illustrated in Scheme 1.

2,2′-(5-Bromo-1,3-phenylene)bis(1-phenyl-1H-benzo[d]-imidazole) (M1). A mixture of 5-bromoisophthalaldehyde (2.10 g, 10.0

DOI: 10.1021/acsami.5b00510
ACS Appl. Mater. Interfaces 2015, 7, 7303−7314

Scheme 1. Synthetic Routes and Chemical Structures of mCP-BPBI and CP-QPBI

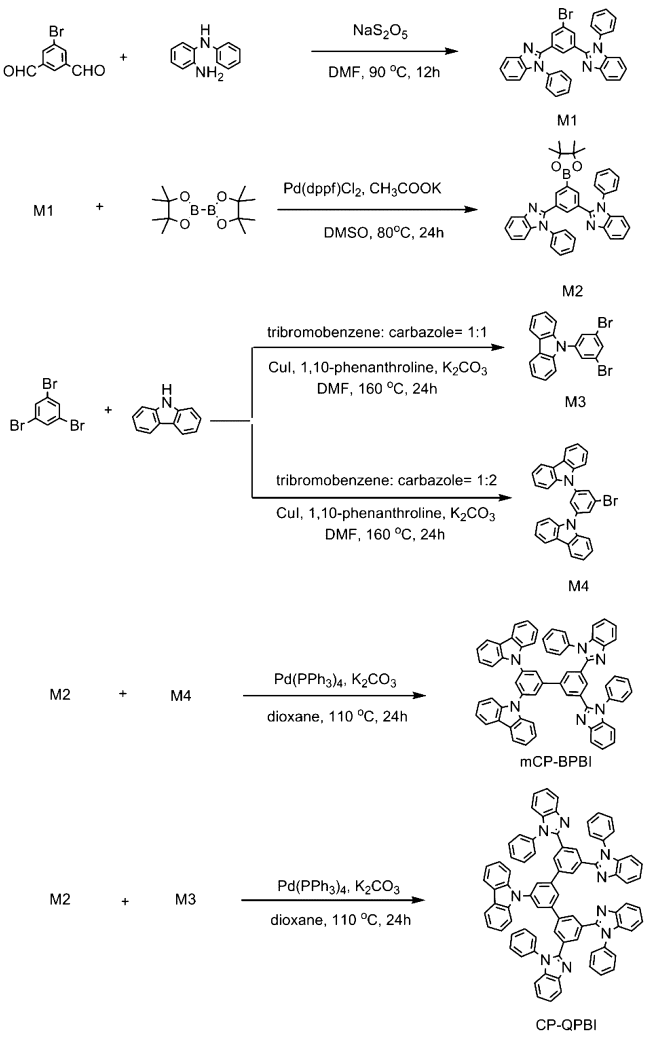

mmol), *N*-phenylbenzene-1,2-diamine (3.73 g, 21.0 mmol), and sodium metabisulfite (3.80 g, 20.0 mmol) was added to 40 mL of DMF. With stirring, the suspension was heated at 80 °C for 12 h. After this mixture cooled, 200 mL of something was added, and the mixture was extracted with 100 mL of ethyl acetate three times. The combined organic layer was dried over anhydrous sodium sulfate. The solvent was removed, and the crude product was purified by silica gel column chromatography with petroleum/ethyl acetate (5:1) as the eluent to give the white solid (3.5 g, 60%).^{1}H NMR (500 MHz, $CDCl_3$): δ 7.86 (s, 1H), 7.84 (d, J = 1.4 Hz, 3H), 7.52 (s, 1H), 7.51−7.42 (m, 6H), 7.34 (t, J = 7.6 Hz, 2H), 7.28 (d, J = 7.5 Hz, 2H), 7.19 (t, J = 6.9 Hz, 6H). ^{13}C NMR (300 MHz, $CDCl_3$, δ): 149.7, 149.4, 137.1, 136.1, 133.3, 130.0, 129.0, 128.4, 127.3, 123.9, 123.4, 122.5, 119.9, 110.6. MS (MALDI-TOF) [m/z]: calcd for $C_{32}H_{21}BrN_4$, 541.44; found, 541.40. Anal. Calcd for $C_{32}H_{21}BrN_4$: C, 70.99; H, 3.91; N 10.35. Found: C, 70.95; H, 3.90; N 10.30%.

2,2′-(5-(4,4,5,5-Tetramethyl-1,3,2-dioxaborolan-2-yl)-1,3-phenylene)bis(1-phenyl-1H-benzo[d]imidazole) (M2). Compound **1** (0.54 g, 1 mmol), Pd(diphenylphosphino ferrocene)Cl_2 (0.06 g, 0.08 mmol), bis(pinacolate)diborane (0.53 g, 2.1 mmol), and anhydrous potassium acetate (0.39 g, 4 mmol) were added to 30 mL of 1,4-dioxane. The mixture was heated at ∼80 °C for 12 h under nitrogen atmosphere. After this mixture cooled to room temperature, 100 mL of ethyl acetate was added to the reaction system, and then the mixture was filtered. Evaporation of the solution was followed by drying with $MgSO_4$. The crude product was purified by silica gel column chromatography (hexanes/ethyl acetate 3:1) to give the white power. ^{1}H NMR (300 MHz, $CDCl_3$, δ): 8.20 (s, 2H), 7.88 (d, J = 7.9 Hz, 2H), 7.50 (s, 1H), 7.41 (t, J = 7.2 Hz, 6H), 7.33 (dd, J = 14.6, 7.3 Hz, 3H), 7.25 (d, J = 5.4 Hz, 3H), 7.16 (d, J = 7.2 Hz, 4H), 1.27 (s, 12H). ^{13}C NMR (300 MHz, $CDCl_3$, δ): 137.2, 129.8, 128.7, 127.4, 119.7, 110.5, 84.0, 24.8. MS (MALDI-TOF) [m/z]: calcd for $C_{38}H_{33}BN_4O_2$, 588.51; found, 588.43. Anal. Calcd for $C_{38}H_{33}BN_4O_2$: C, 77.55; H, 5.65; N 9.52. Found: C, 77.45; H, 5.70; N 9.56%.

9-(3,5-Dibromophenyl)-9H-carbazole (M3). Carbazole (5.6 g, 35 mmol), 1,3,5-tribromobenzene (10 g, 31 mmol), K_2CO_3 (4.9 g, 35 mmol), copper(I) iodide (0.06 g, 3 mmol), and 1,10-phenanthroline (0.06 g, 3 mmol) were added to 100 mL of dried DMF. The mixture was heated at 160 °C for 12 h under nitrogen atmosphere. After this mixture cooled to room temperature, the reaction was quenched with 200 mL of water and extracted with 100 mL of dichloromethane three times. Combining the organic layer and removing the solvent, the residue was then purified by silica gel column chromatography with petroleum ether/ethyl acetate (10:1) as the eluent to give 7.78 g of white power. ^{1}H NMR (600 MHz, $CDCl_3$, d): 8.13 (d, J = 7.5 Hz, 2 H), 7.75 (s, 1 H), 7.70 (s, 2 H), 7.54−7.25 (m, 6 H). MS (ESI) [m/z]: calcd for $C_{18}H_{11}Br_2N$, 401.09; found, 401.00. Anal. Calcd for $C_{18}H_{11}Br_2N$: C, 53.90; H, 2.76; N 3.49. Found: C, 53.82; H, 2.84; N 3.53%.

9,9′-(5-Bromo-1,3-phenylene)bis-9H-carbazole (M4). The synthetic method of M4 was according to that of M3 with a yield of 42.6%. ^{1}H NMR(300 MHz, $CDCl_3$, d): 8.13 (d, J = 8.2 Hz, 4 H), 7.84 (s, 2 H), 7.77 (s, 1 H), 7.53 (d, J = 8.2 Hz, 4 H), 7.45 (t, J = 7.2 Hz, 4H), 7.32 (t, J = 7.2 Hz, 4 H). MS (ESI) [m/z]: calcd for $C_{30}H_{19}BrN_2$, 487.39; found, 487.32. Anal. Calcd for $C_{30}H_{19}BrN_2$: C, 73.93; H, 3.93; N 5.75. Found: C, 73.88; H, 3.92; N 5.56%.

9,9′-(3′,5′-Bis(1-phenyl-1H-benzo[d]imidazol-2-yl)biphenyl-3,5-diyl)bis(9H-carbazole) (mCP-BPBI). M2 (0.58 g, 1.0 mmol), M4 (0.57 g, 1.2 mmol), Pd[$P(C_6H_5)_3]_4$ (0.14 g, 0.15 mmol), and aqueous KH_2PO_4 solution (2 N, 10 mL) were added to a 250 mL three-necked flask containing 1,4-dioxane (50 mL). The mixture was heated to 110 °C under nitrogen atmosphere for 24 h. After this mixture cooled, 100 mL of water was added to the reaction mixture, which was then extrated with CH_2Cl_2. Evaporation of the solution was followed by drying with $MgSO_4$. The crude product was purified by silica gel column chromatography with $CHCl_3$ as the eluent to give a white solid (0.65 g, 75%). ^{1}H NMR (300 MHz, $CDCl_3$, δ): 8.59 (s, 1H), 8.23 (d, J = 7.6 Hz, 4H), 7.89 (d, J = 7.8 Hz, 2H), 7.73 (s, 1H), 7.54−7.44 (m, 6H), 7.44−7.27 (m, 12H), 7.24−7.15 (m, 6H), 7.08−6.91 (m, 6H), 6.56 (t, J = 7.5 Hz, 2H). ^{13}C NMR (75 MHz, $CDCl_3$, δ): 142.67, 140.50, 139.65, 138.11, 136.33, 130.63, 129.80, 128.63, 127.21, 126.04, 124.54, 124.20, 123.67, 123.45, 123.16, 120.36, 120.32, 119.86, 110.38, 109.66. MS (MALDI-TOF) [m/z]: calcd for $C_{62}H_{40}N_6$, 869.0; found, 869.2. Anal. Calcd for $C_{62}H_{40}N_6$: C, 85.69; H, 4.64; N 9.67. Found: C, 85.65; H, 4.72; N 9.59%.

9-(3,5-Bis(3,5-bis(1-phenyl-1H-benzo[d]imidazol-2-yl)phenyl)-9H-carbazole (CP-QPBI). The synthetic method of CP-QPBI was according to mCP-BPBI with a yield of 45%. ^{1}H NMR (300 MHz, $CDCl_3$, δ): 8.28 (d, J = 7.5 Hz, 2H), 8.09 (s, 2H), 7.89 (d, J = 7.8 Hz, 2H), 7.71 (s, 2H), 7.55−7.14 (m, 35H), 7.01 (t, J = 6.8 Hz, 4H), 6.91 (s, 2H). ^{13}C NMR (75 MHz, $CDCl_3$, δ): 150.78, 142.23, 141.93, 140.87, 139.51, 138.48, 136.95, 136.37, 130.67, 129.90, 129.72, 129.09, 128.82, 127.27, 125.85, 125.33, 124.30, 123.58, 123.19, 123.08, 120.23, 119.99, 119.81, 110.39, 109.86. MS (MALDI-TOF) [m/z]: calcd for $C_{82}H_{53}N_9$, 1164.3; found, 1164.3. Anal. Calcd for $C_{82}H_{53}N_9$: C, 84.59; H, 4.59; N 10.83. Found: C, 84.55; H, 4.76; N 10.88%.

3. RESULTS AND DISCUSSION

Synthesis and Characterization. The synthetic routes and chemical structures of the novel bipolar hosts are shown in Scheme 1. First, 2,2′-(5-bromo-1,3-phenylene)bis(1-phenyl-1*H*-benzo[d]imidazole) (M1) was prepared from 5-bromoisophthalaldehyde and *N*-phenylbenzene-1,2-diamine catalyzed by sodium metabisulfite in DMF, which then converted to 2,2′-(5-(4,4,5,5-tetramethyl-1,3,2-dioxaborolan-2-yl)-1,3-phenylene)bis(1-phenyl-1*H*-benzo[*d*]imidazole) (M2) cata-

DOI: 10.1021/acsami.5b00510
ACS Appl. Mater. Interfaces 2015, 7, 7303−7314

lyzed by $PdCl_2$(dppf). The starting materials M3 and M4 were synthesized by the classic Ullmann reaction of carbazole and 1,3,5-tribromobenzene. The target compounds mCP-BPBI and CP-QPBI were prepared from M3 and M4 by the Suzuki cross-coupling reactions with the aryboronic ester. All the materials were purified by column chromatography on silica gel before device fabrication. ^{1}H and ^{13}C NMR spectroscopy, mass spectrometry, and elemental analysis were used to characterize the molecular structures.

Thermal Properties. TGA and DSC were employed to investigate the thermal properties of mCP-BPBI and CP-QPBI. According to Figure 1, the two compounds shown very high

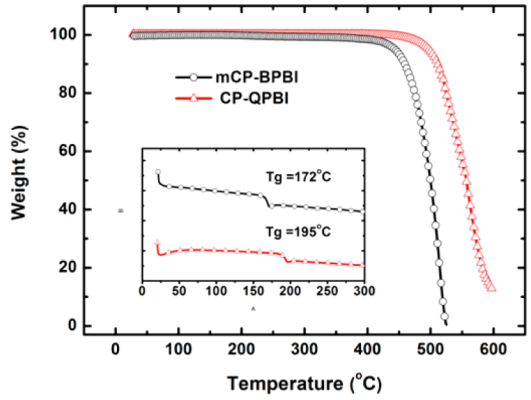

Figure 1. TGA curves of mCP-BPBI and CP-QPBI. (inset) Corresponding DSC traces.

thermal-decomposition temperatures (T_d, corresponding to 5% weight loss) of 443 °C (mCP-BPBI) and 500 °C (CP-QPBI). Such high T_d should be attributed to the meta-position linking induced bulky backbone structure, which is significantly beneficial to the thermal stability of the material. In addition, the DSC curves record well-defined glass-transition temperatures (T_g) of 172 °C (mCP-BPBI) and 195 °C (CP-QPBI) during the second heating scans. As a result, these two hosts could form homogeneous and amorphous films upon solution processing, which verified by AFM images the spin-coated thin films (Figure 2). No aggregation and crystallization were

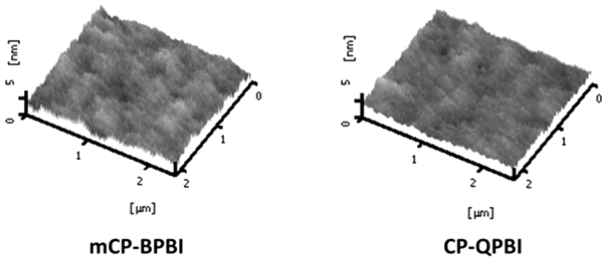

Figure 2. AFM topographic images of mCP-BPBI and CP-QPBI.

observed, and the root-mean-square (RMS) roughness values are 0.45 (mCP-BPBI) and 0.34 (CP-QPBI). These values indicate that the increase of the benzimidazole moieties strongly enhances the film-forming ability and morphological stability of the host material, which could suppress the potential phase speration and improve the device performance during opreation.

Photophysical Properties. The absorption, fluorescence, and low-temperature phosphoresence spectra of mCP-BPBI and CP-QPBI are shown in Figure 3. Related thermal and photophysical data are collected in Table 1. Because of the

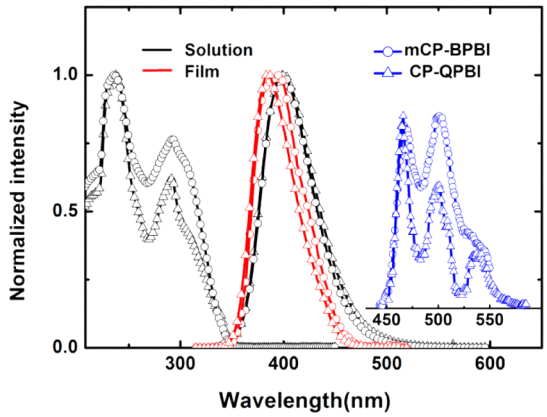

Figure 3. Room-temperature absorption and emission spectra of mCP-BPBI and CP-QPBI and low-temperature phosphorescence spectra at 77 K.

structural similarity of these bipolar host materials, the photophysical properties of the two compounds are similar. The strong absorption peaks at 236 nm can be attributed to their $\pi-\pi^*$ transitions, while the absorptions at ~291 and 305 nm correspond to the carbazole- and benzimidazole-centered $n-\pi^*$ transitions, respectively. Besides, a weak absorption shoulder at 338 nm, which was not found in CP-QPBI, can be attributed in the case of mCP-BPBI to the weak intramolecular charge transfer (ICT) between carbazole and benzimidazole. Upon photoexcitation at the absorption maximums at room temperature, the fluorescence spectra of mCP-BPBI and CP-QPBI are nearly identical to each other both in solution (401/398) and film (395/387). These observations suggest that the delocalization of the excited states do not obviously extend to the increased peripheral benzoimidazole units. In addition, the narrowing of half peak width and the small blue shift in the solid PL spectra compared with the solution ones of the two compounds reflect that the introduction of benzoimidazole units to the meta positions of the twisted terphenyl core further induce the molecule to a nonplanar three-dimensional structure, which can effectively inhibit the unwanted intermolecular interaction. Moreover, the low-temperature phosphorescence spectra were measured at 77 K in dichloromethane, and the triplet energies were both 2.68 eV for these two compounds. To prevent reverse energy transfer from guest, the bipolar host that contains donor and acceptor units should avoid strong ICT effect to give triplet energy higher than the phosphor. The increased numbers of benzoimidazole unit do not reduce the triplet energy of CP-QPBI, which may be attributed to the meta−meta configuration and the molecular rigidity induced by steric hindrance, and that is beneficial for suppressing the ICT effect and decreasing the structure relaxation-induced excited-energy loss.

This hypothesis is supported by the relatively weak solvent-dependent shift in the emission spectrum depicted in Figure 4. The change in dipole moment between the excited and ground states can be estimated by the Lippert−Mataga equation (eq 1), which expresses the Stokes shift as a function of the solvent polarity parameter $\Delta f(\varepsilon, n)$.[38]

DOI: 10.1021/acsami.5b00510
ACS Appl. Mater. Interfaces 2015, 7, 7303−7314

Table 1. Physical Properties of the Compounds

	T_g/T_d[a] [°C]	λ_{abs}[b] [nm]	λ_{em}[b] [nm]	λ_{em}[c] [nm]	E_T[d] [eV]	E_{ox}[e] [V]	E_{red}[e] [V]	HOMO[f] [eV]	LUMO[f] [eV]	E_g[g] [eV]
mCP-BPBI	172/443	335, 291, 235	401	395	2.68	0.83	−2.61	−5.63	−2.18	3.45
CP-QPBI	195/500	292, 236	398	387	2.68	0.78	−2.33	−5.58	−2.47	3.11

[a]T_d, corresponding to 5% weight loss. [b]Measured in CH_2Cl_2 solutions. [c]Measured in neat film. [d]Estimated from the onset of phosphorescence in the CH_2Cl_2 glass at 77 K. [e]The onset potential. [f]Determined using cyclic voltammetry. [g]E_g was calculated from the different value of HOMO and LUMO.

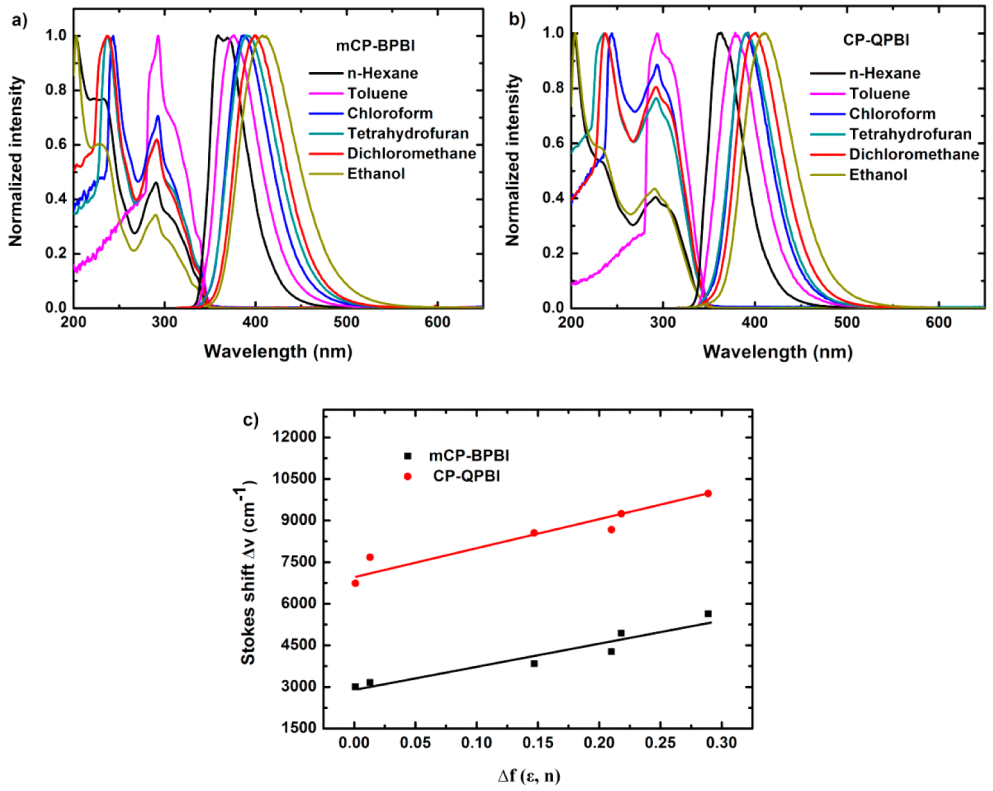

Figure 4. PL spectra of mCP-BPBI (a) and CP-QPBI (b) in different solvents. (c) Lipperte−Mataga plot of mCP-BPBI and CP-QPBI in various solutions.

Table 2. Spectral Properties of mCP-BPBI and CP-QPBI in Different Solvents

		mCP-BPBI			CP-QPBI		
solvents	Δ_f[a] (ε, n)	λ_{abs}[b] (nm)	λ_f[c] (nm)	ΔV[d] (cm^{-1})	λ_{abs}[b] (nm)	λ_f[c] (nm)	ΔV[d] (cm^{-1})
n-hexane	0.001	333, 290, 233	359, 370	3003	291, 233	362	6739
toluene	0.013	336, 292	376	3166	293	378	7674
chloroform	0.147	337, 292, 243	387	3834	293, 244	391	8554
tetrahydrofuran	0.210	335, 291, 237	391	4275	292, 236	391	8671
dichloromethane	0.218	334, 291, 237	400	4940	292, 235	400	9246
ethanol	0.289	333, 290, 230	410	5639	291, 233	410	9974

[a]Δ_f is the orientation polarizability parameter of the solvent. [b]λ_{abs} is absorption wavelength. [c]λ_f is fluorescent wavelength. [d]ΔV is the Stokes shift.

$$\Delta\nu = \nu_{abs} - \nu_f \cong \frac{2(\Delta\mu)^2}{hca^3}\Delta f(\varepsilon, n) + A \quad (1)$$

and $\Delta f(\varepsilon, n)$ is calculated by

$$\Delta f(\varepsilon, n) = \frac{\varepsilon - 1}{2\varepsilon + 1} - \frac{n^2 - 1}{2n^2 + 1} \quad (2)$$

Here, ε and n are the static dielectric constant and refractive index of the solvent, respectively. In eq 1, $\Delta\nu$ means the Stokes shift between absorption and fluorescence, h is the Planck's constant, a represents the solute cavity radius, and c is the velocity of light.[39] Figure 4 shows the plots of Δf as a function of $\Delta\nu$ with the slope values of 11 232 and 9152 cm^{-1} for mCP-BPBI and CP-QPBI. Related spectral data are in Table 2. Accordingly, the calculated $\Delta\mu$ values were only 9.92 and 9.56 D, which are consistent with the weak ICT trends of the two hosts. Furthermore, small molecular dipole moment could weaken the intermolecular electric field and enhance the carrier mobility of the organic thin film due to the low dipolar disorder, which facilitates the charge balance in the electroluminescent devices.[37]

Electrochemical Properties and Density Functional Theory Simulation. The electrochemical behaviors of the two

DOI: 10.1021/acsami.5b00510
ACS Appl. Mater. Interfaces 2015, 7, 7303−7314

hosts were investigated by CV using tetrabutylammonium hexafluorophosphate ($TBAPF_6$) as the supporting electrolyte in anhydrous DMF for cathodic scans and CH_2Cl_2 for anodic sweeping. Figure 5 shows that both compounds have distinct

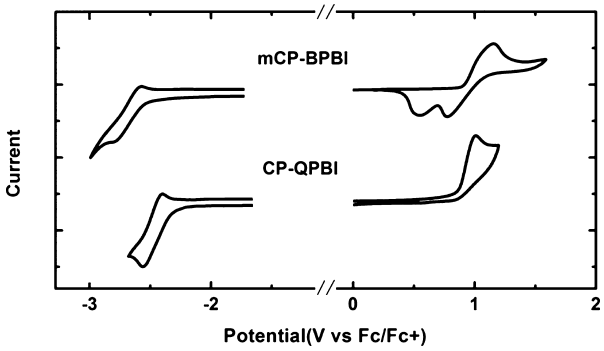

Figure 5. Cyclic voltammogram of mCP-BPBI and CP-QPBI.

oxidation and reduction behaviors, which clearly indicate their potential in bipolar carrier transporting. According to the onset potentials, we calculated the highest occupied molecular orbital (HOMO) and the lowest unoccupied molecular orbital (LUMO) energy levers of mCP-BPBI and CP-QPBI to be −5.63/−2.18 eV and −5.58/−2.47 eV, respectively. The similar HOMO levels are due to the small interaction between the donor and acceptor units, which induced the HOMO of the two compounds similar to carbazole. On the other hand, the increased electron-withdrawing benzoimidazole unit deepens the LUMO of CP-QPBI, which indicates the electron-injection to EML should be improved in the OLEDs. On the basis of the CV results, the energy gaps in mCP-BPBI and CP-QPBI were estimated as 3.45 and 3.11 eV, which is consistent with the results calculated from the optical absorption edges. In addition, DFT calculations were performed to systematically investigate the influence of the molecular structure on the electronic properties. The optimized structure and the HOMO/LUMO distribution for mCP-BPBI and CP-QPBI are given in Figure 6. The LUMOs of the two compounds are localized primarily on the electron-deficient benzimidazole fragments, while the HOMOs are mostly distributed over the electron-rich carbazole units. The dihedral angles of the electron donor and acceptor are 36.9°, and 56.8°, respectively. This finding also confirms the minimal intramolecular interactions in the two hosts, because the twist configuration can effectively reduce the charge transfer from the carbazole moiety to the benzimidazole moiety. The complete separation of HOMO and LUMO was preferable for the transporting of both hole and electron, which enables the charge-balance properties of these hosts. Furthermore, the T_1 states of these two molecules were also simulated to obtain the spin-density distribution (SDD), which indicates the locations of the T_1 excited states. According to the contours of the SDD, the T_1 states of mCP-BPBI and CP-QPBI are absolutely contributed by benzimidazole unit (see Figure 6). Therefore, the incorporation of more benzimidazole moieties did not induce the shift of the T_1 to the biphenyl group, which is consistent with the optical experimental values that both hosts possess the same triplet energy. As the combined result, we successfully realized the effectively enhanced electron injection/transporting ability without losing the triplet energy by turning the molecular configurations of the hosts.

Reorganization Energy. To understand the charge-transport abilities of mCP-BPBI and CP-QPBI, systematic evaluation of the reorganization energy (λ), which reflects the geometry relaxation energies of one molecule going from the neutral state to the charged state, was extremely important. The reorganization energies for both electron and hole of the two hosts were calculated at the B3LYP/6-31G(d) level.[40] Adopting the general hypothesis, the charge-transport process of organic thin film was found to show a hopping-type behavior, and the reaction between adjacent segments can be described as follows:

$$M^{+/-} + M^* \rightarrow M^* + M^{+/-} \quad (3)$$

In which $M^{\pm}$ indicates the molecule in a cationic or anionic state. M* is a neighboring molecule in a neutral state.[41] Accordingly, the corresponding charge-transfer rate (k_{CT}) can be approximately described by Marcus' equation (eq 4), if the vibrational mode was guaranteed to be classical by temperature.

$$k_{CT} = \frac{4\pi^2}{h} H_{AB}{}^2 \frac{1}{\sqrt{4\pi\lambda k_B T}} \exp\left(-\frac{\lambda}{4k_B T}\right) \quad (4)$$

where h is the Planck constants, H_{AB} is the charge-transfer integral, k_B is the Boltzmann constant, and T is the temperature. In amorphous organic solids, H_{AB} can be expected to constitute a less variable quantity due to the random packing of molecules. Thus, the charge-transfer rate should be mainly

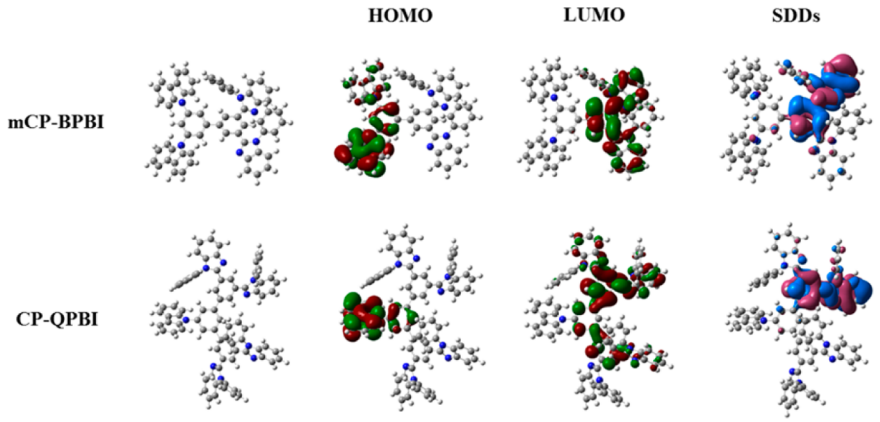

Figure 6. DFT calculations of the molecular configurations in the ground states and the spin-density distributions in the T_1 states of mCP-BPBI and CP-QPBI.

DOI: 10.1021/acsami.5b00510
ACS Appl. Mater. Interfaces 2015, 7, 7303−7314

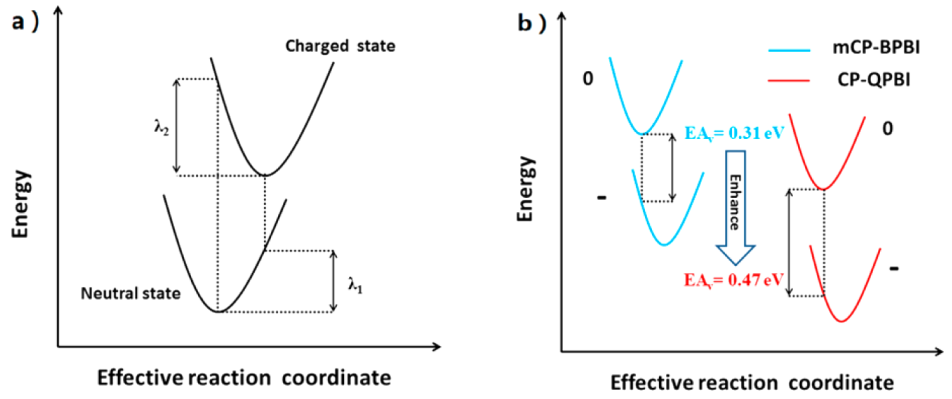

Figure 7. (a) Sketch of the reorganization energy calculation. (b) Description of the electron affinity of mCP-BPBI and CP-QPBI.

determined by the key parameter λ. According to eq 4, a low λ value is necessary for an efficient charge-transport process. The reorganization energy for hole/electron transfer is defined as follows:

$$\lambda^+ = \lambda_1 + \lambda_2 = \mathrm{IP_v} - \mathrm{HEP} \quad (5)$$

$$\lambda^- = \lambda_1 + \lambda_2 = \mathrm{EEP} - \mathrm{EA_v} \quad (6)$$

where HEP and EEP represent the hole- and electron-extraction potentials, respectively. The $\mathrm{IP_v}$ and $\mathrm{EA_v}$ are the ionization potential and the electron affinity, respectively.[42,43] It is generally considered that the IP together with EA can be used to weigh the hole- and electron-injection abilities of the host, respectively. When EA is large and IP is small, electron and hole can be easily injected into the materials. Figure 7 schematically illustrated the classical calculation of the reorganization energy and specific enhancement of electron affinity based on the hopping model.

In addition, the balanced electron and hole transportation play an important role in efficient charge recombination. When we assume $H^+_{AB} = H^-_{AB}$ in eq 4, the ratio of the hole- and electron-transfer rate can be obtained as follows.[44,45]

$$\frac{k^+}{k^-} = \left(\frac{\lambda^-}{\lambda^+}\right)^{1/2} \exp\left(\frac{\lambda^- - \lambda^+}{4k_BT}\right) \quad (7)$$

The calculated $\mathrm{IP_v}$, $\mathrm{EA_v}$, λ^+, λ^-, and k^+/k^- values are listed in Table 3. Compared with mCP-BPBI, whose EA value is 0.31 eV, CP-QPBI has much larger EA value of ~0.47 eV. Thus, according to the relationship between EA and the charge-injection property, it is easy to conclude that the electron-injection ability was improved greatly with the introduction of more benzimidazole groups. Besides, the reorganization energy of mCP-BPBI and CP-QPBI for hole λ^+ is 0.08 and 0.11 eV, while for electron λ^- it is 0.39 and 0.22 eV, respectively. The two hosts show high charge mobility of both hole and electron due to their low reorganization energy.[46,47] The slight deference of λ^+ would suggest that the hole mobility of the two hosts are similar. In contrast, the λ^- of CP-QPBI is much smaller than that of mCP-BPBI, which indicates that the increased benzimidazole units significantly enhance the electron-transport property of CP-QPBI. More importantly, the calculated ratio of hole- and electron-transfer rate k^+/k^- for CP-QPBI (4.2) is extremely small when compared to that for mCP-BPBI (38.8), which means the host CP-QPBI possesses a more balanced charge transition of hole and electron. From these results, we found that the charge injection/transport is determined mainly by the moieties contributing predominantly to its molecular orbital. Therefore, by controlling the major contributors to the donor and acceptor units, a systematic design of bipolar host materials for efficient PHOLEDs with desirable charge-transport properties can be achieved.

Table 3. Reorganization Energies for Hole Transfer and Electron Transfer Calculated by DFT B3LYP/6-31G(d)

host	$\mathrm{IP_v}$, eV	HEP, eV	$\mathrm{EA_v}$, eV	EEP, eV	λ^+, eV	λ^-, eV	k^+/k^-
mCP-BPBI	6.42	6.33	0.31	0.69	0.09	0.39	38
CP-QPBI	6.38	6.27	0.47	0.69	0.11	0.22	4

Single Carrier Devices. The charge-injection and charge-transport properties of mCP-BPBI and CP-QPBI in actual solution-processed thin film were further investigated by single-carrier dominant devices. The structure of electron-only devices are ITO/solution-deposited bipolar hosts (100 nm)/Cs_2CO_3/Al, and the hole-only devices are ITO/PEDOT:PSS/solution-deposited bipolar hosts (100 nm)/Al. Because of the large energy barrier between the HOMOs of the bipolar hosts (5.63 eV for mCP-BPBI and 5.58 eV for CP-QPBI) and the work function of ITO (Φ_f = 4.5 eV), the hole-injection in the electron-dominant devices was assumed to be suppressed. Similarly, the electron-injection in the hole-dominant devices was also considered to be prevented by the large barrier between the LUMOs of the bipolar hosts (2.18 eV for mCP-BPBI and 2.47 eV for CP-QPBI) and the work function of Al (Φ_f = 4.2 eV). As seen in Figure 8, both hole- and electron-dominant devices exhibit significant currents, which indicate the bipolar charge-transport properties of mCP-BPBI and CP-QPBI. In addition, the electron current density of the CP-QPBI was much higher than that of the mCP-BPBI, which matches well with the calculated large electron affinity and low electron reorganization energy of CP-QPBI. These results clearly demonstrate that the electron-transport and -injection abilities are significantly enhanced by increasing benzoimidazole units in the bipolar host.

Electroluminescent Properties. To estimate the applicability of the two compounds as solution-processable bipolar hosts, we first examined the performance of $Ir(mppy)_3$-based single-layer green electrophosphorescent device A with the simple configuration of ITO/PEDOT:PSS (40 nm)/host:$Ir(mppy)_3$ (12 wt %, 100 nm)/Cs_2CO_3 (1 nm)/Al(100 nm). The relative energy level of the material is shown in Figure 10. In these devices, PEDOT:PSS and Cs_2CO_3 served as the hole- and electron-injection layers, while ITO and Al were used as

DOI: 10.1021/acsami.5b00510
ACS Appl. Mater. Interfaces 2015, 7, 7303−7314

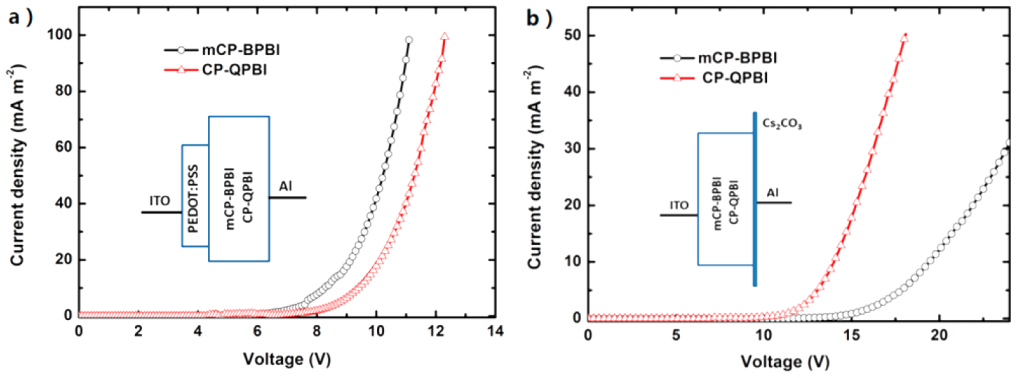

Figure 8. Current density−voltage (J−V) characteristics of carrier-only devices: (a) hole only and (b) electron only.

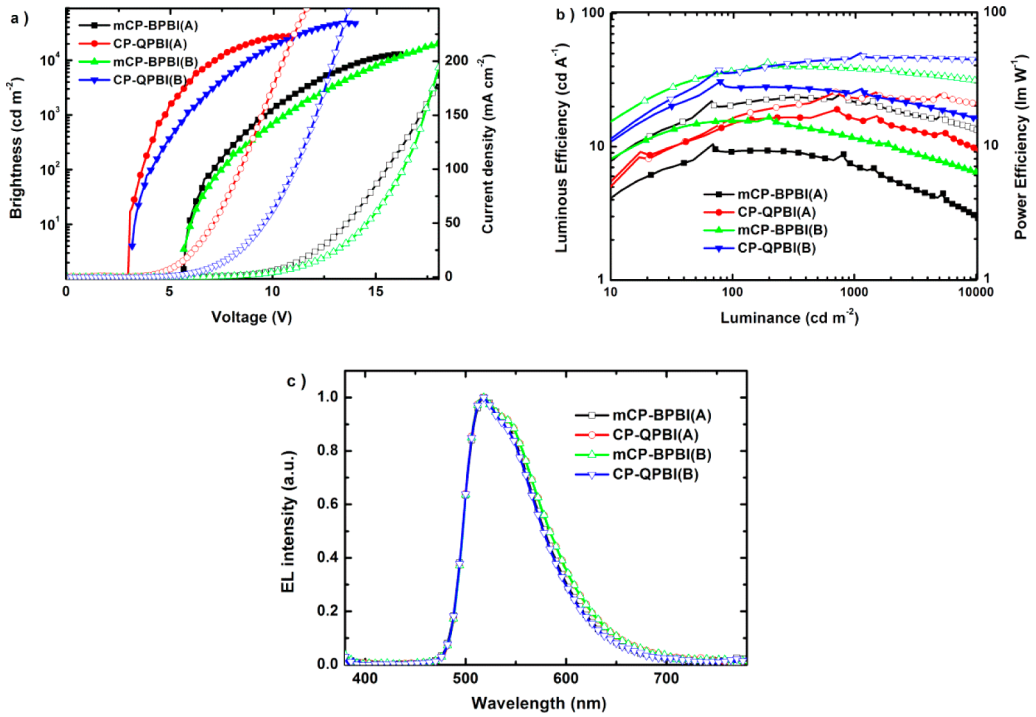

Figure 9. (a) Current density (hollow)−voltage−brightness (solid) (J−V−B) curves. (b) Luminous efficiency (hollow) and power efficiency (solid) as a function of brightness. (c) EL spectra of green-emitting devices.

Table 4. Device Performances of the PHOLEDs

device	host	V_{on} [V]	$\eta_{c,max}$ [cd A^{-1}]	$\eta_{p,max}$ [lm W^{-1}]	at 100 cd m^{-2} [V]/[cd A^{-1}]/[lm W^{-1}]	at 1000 cd m^{-2} [V]/[cd A^{-1}]/[lm W^{-1}]	at 10 000 cd m^{-2} [V]/[cd A^{-1}]/[lm W^{-1}]	CIE [x, y]
A(green)	mCP-BPBI	5.7	25.3	10.2	7.1/20.9/9.1	9.6/21.9/7.1	14.6/13.4/2.9	(0.31, 0.60)
A(green)	CP-QPBI	2.9	26.1	18.7	3.7/16.7/15.0	4.8/25.5/16.6	7.0/21.1/9.4	(0.30, 0.60)
B(green)	mCP-BPBI	5.7	42.6	16.3	7.5/37.2/15.4	10.6/38.4/11.2	15.7/31.3/6.2	(0.31, 0.60)
B(green)	CP-QPBI	3.3	47.5	27.8	4.2/36.4/27.2	5.8/46.7/24.7	8.9/45.1/15.6	(0.31, 0.60)
A(blue)	mCP-BPBI	7.6	6.8	2.0	9.5/5.2/1.7	12.5/5.5/1.4	−/−	(0.16, 0.32)
A(blue)	CP-QPBI	4.6	9.4	3.9	6.2/5.4/2.7	7.9/9.3/3.7	−/−	(0.16, 0.32)
B(blue)	mCP-BPBI	7.7	16.3	5.1	8.5/8.7/3.7	9.6/16.3/5.2	−/−	(0.16, 0.33)
B(blue)	CP-QPBI	4.8	17.8	8.2	6.9/15.5/7.0	9.0/17.0/6.0	−/−	(0.16, 0.33)

the anode and cathode, respectively. Figure 9 shows the current density−voltage−brightness (J−V−B) characteristics, the curves of luminous and power efficiency versus brightness, and the EL spectra of the devices. Table 4 lists the key characteristics of the devices. Both devices show typical green emission at ∼530 nm that originates from the guest Ir(mppy)$_3$, indicating a complete energy transfer from the bipolar host to the gust. Device A with mCP-BPBI as host displays a turn-on voltage of 5.7 V, a maximum luminous efficiency of 25.3 cd A^{-1}, and a maximum power efficiency of 10.2 lm W^{-1}. Compared to the reported triphenylamine-based host matials,[7] the enhanced performance of mCP-BPBI can be attributed to its bipolar transporting property and suitable energy levels for efficient charge injection. In addition, the sufficiently high triplet energy

DOI: 10.1021/acsami.5b00510
ACS Appl. Mater. Interfaces 2015, 7, 7303−7314

of mCP-BPBI (2.68 eV) can successfully confine the excitons and suppress triplet energy back-transfer from the phosphorescent emitter, thus also leading to an improved efficiency. Similarly, the corresponding solution-processed green PHOLEDs using the more electron-transport CP-QPBI as host endowed the device with extremely low driving voltage of 2.9 V for onset, 3.5 V for 100 cd m^{-2}, 3.8 V for 1000 cd m^{-2}, and 4.5 V for 10 000 cd m^{-2}, respectively. As far as we know, the turn-on voltage of 2.9 V is the lowest value in $Ir(mppy)_3$-based solution-processed PHOLEDs without p- or n-doping layer, and this value almost reaches the theoretical limit of the energy gap voltage for the emitter. Moreover, the low operating voltage enables the device to reach a high power efficiency of 18.7 lm W^{-1}, which is already equivalent to those of the multilayer PHOLEDs using TPBI as the ETL.[32,49] These performances are better than the previously reported $Ir(mppy)_3$-based solution-processed single-layer PHOLEDs utilizing the carbazole-based dendrimer or PVK polymer as soluble hosts (Table 5).[1,50] For further enhancing the performance, a thin TPBI layer was inserted between the EML and the cathode; Figure 10 shows the energy level diagram of the multilayer device B with the configuration of ITO/PEDOT:PSS (40 nm)/host:$Ir(mppy)_3$ (12 wt %,40−50 nm)/TPBI (40 nm)Cs_2CO_3 (1 nm)/Al (100 nm). In comparison with the single-layer devices, the luminance of device B was greatly enhanced, although the turn-on voltage was unchanged. Importantly, because of the inhibition of the cathode quenching effect, the maximum luminous and power efficiency of the CP-QPBI-based devices were significantly improved to 47.5 cd A^{-1} and 27.8 lm W^{-1}, respectively. These performances are among the highest levels in the scientific literature of solution-processed green PHOLEDs.[51,52] Efficiency roll-off at higher luminence was also observed, which is typical in PHOLEDs. At the practical brightness of 1000 cd m^{-2}, the luminous and power efficiencies of CP-QPBI-based device remain above 46 cd A^{-1} and 24 lm W^{-1}, respectively. Even at the brightness as high as 10 000 cd m^{-2}, the luminous efficiency also remains as high as 45.1 cd A^{-1}. The remarkably low operating voltage and efficiency roll-off can be attributed to the excellent electron-transport characteristics and balanced charge-combination properties of CP-QPBI, which can significantly reduce the resistance of the device and broaden the recombination zero to minimize the number of possible quenching pathways and avoiding charge-carrier loss. We also note that mCP-BPBI-based device showed the maximum luminous efficiency value and power efficiency at low brightness (280 cd m^{-2}), whereas the device with CP-QPBI as host showed the high efficiency at high brightness (5640 cd m^{-2}), which clearly demonstrates the significance of excellent electron injecting and transporting in affecting the charge recombination in the solution-processed devices.

Table 5. Device Performances of Solution-Processed Green PHOLEDs

device configration	V_{on} [V]	$\eta_{c,max}$ [cd A^{-1}]	$\eta_{p,max}$ [lm W^{-1}]	reference
ITO/PEDDT/CP-QPBI:$Ir(mppy)_3$/Cs_2CO_3/Al	2.9	26.1	18.7	this work
ITO/PEDDT/G3:$Ir(ppy)_3$/TPBI/LiF/Al	4.8	20.7	8.6	32
ITO/PEDDT/DM-TIBN:$Ir(ppy)_3$/BCP:Cs/Al	6.9	27.3	7.3	48
ITO/PEDDT/TBBI:$Ir(ppy)_3$/BCP:Cs/Al	13.1	27.4	4.4	7
ITO/PEDDT/CP-QPBI:$Ir(mppy)_3$/TPBI/Cs_2CO_3/Al	3.3	47.5	27.8	this work
ITO/PEDDT/TCTA/PVK:CBP:$Ir(mppy)_3$/TPBI/LiF/Al	3.0	27.2	17.8	50
ITO/PEDDT/G3:OXD7:$Ir(ppy)_3$/TPBI/LiF/Al	3.8	36.3	18.5	32
ITO/PEDDT/Allyl-TFB/26DCzPPy:$Ir(mppy)_3$/TPBI/CsF/Al	3.1	31.4	21.8	49
ITO/PEDDT/PVK:OXD7:$Ir(ppy)_3$/TPBI/LiF/Al	5.0	27.7	9.5	32
ITO/TCzII/P1:P2:$Ir(pppy)_3$/BCP/LiF/Al	6.5	48.4	18.2	51
ITO/PEDDT/X-TAPC/X-H2:X-$Ir(mppy)_3$/TPBI/CsF/Al	3.0	50.0	30.0	52

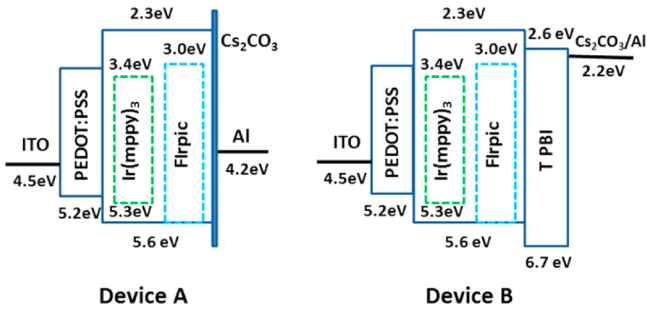

Figure 10. Schematic energy-level diagram of devices A and B.

To verify our concept, we also fabricated blue electrophosphorescent devices with mCP-BPBI and CP-QPBI as the hosts; except for the different dopant (FIrpic) and concentration (10 wt %), the structures were similar to that of the green-emitting one. The EL performances were also displayed in Table 4, and the spectra were shown in Figure 11. Blue-emitting single active-layer PHOLEDs with solution-processed mCP-BPBI showed a turn-on voltage of 7.6 V, a maximum luminous efficiency of 6.8 cd A^{-1}, and a maximum power efficiency of 2.0 lm W^{-1}, while the device using CP-QPBI as host exhibited a turn-on voltage of 4.6 V, a maximum luminous efficiency of 9.4 cd A^{-1}, and a maximum power efficiency of 3.9 lm W^{-1}. Clearly, CP-QPBI-based EML also significantly reduces the turn-on voltage of the blue PHOLEDs, and the driving voltage at 100 and 1000 cd m^{-2} became also 3−4 V lower than that of mCP-BPBI-based EML. After insertion of TPBI layer to control the diffusion of the triplet excitons, the maximum luminance and power efficiency of CP-QPBI-based device were significantly enhanced to 17.8 cd A^{-1} and 8.2 lm W^{-1}, respectively. Although these performances are moderate relative to the highest values reported for solution-processed FIrpic-based PHOLEDs, the distinctly reduced operating voltage (9.5 V for mCP-BPBI and 6.2 V for CP-QPBI) and simultaneously enhanced power efficiency (5.1 lm W^{-1} for mCP-BPBI and 8.2 lm W^{-1} for CP-QPBI) strongly demonstrate that even for the blue PHOLEDs, the charge recombination and radiative transition were also mainly determined by the balanced carrier injection and transporting properties of the bipolar hosts. It is worth noting that, similar to $Ir(mppy)_3$-doped device, blue PHOLEDs using CP-QPBI as host also achieve its highest efficiency at high brightness (1100 cd m^{-2}). Usually, the efficiency of the single active-layer PHOLEDs entirely depends on the performance of the host. Thus, the remarkably decreased operating voltage and the highest efficiency achieved at high brightness in both blue and

DOI: 10.1021/acsami.5b00510
ACS Appl. Mater. Interfaces 2015, 7, 7303−7314

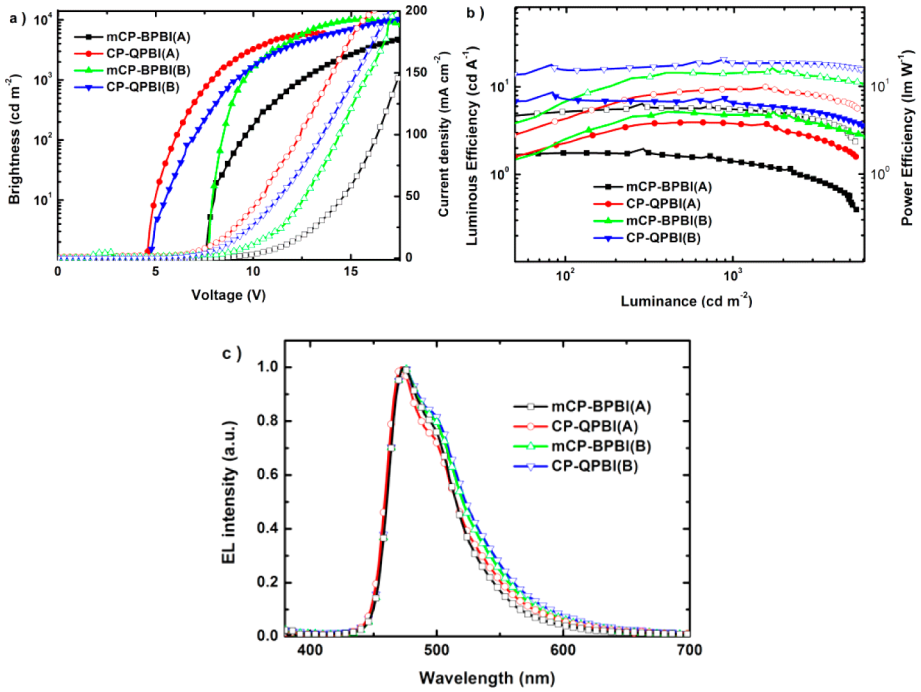

Figure 11. (a) Current density (hollow)−voltage−brightness (solid) (J−V−B) curves. (b) Luminous efficiency (hollow) and power efficiency (solid) as a function of brightness. (c) EL spectra of blue-emitting devices.

green devices strongly prove the balanced charge transfer and efficient exciton recombination in the bipolar host with multielectron transport moieties. These results also imply that the strategy applied to improve electron transport and charge balance of the EML by tuning the ratio of donor and acceptor units is a promising approach for the construction of desirable host for high-performance PHOLEDs.

4. CONCLUSION

In summary, two bipolar host materials, namely, mCP-BPBI and CP-QPBI, composed of electron-donating carbazole and electron-accepting benzimidazole linked to the meta position of the phenyl core, have been synthesized and characterized. The twisted configuration effectively inhibits the direct electronic interaction between the donor and acceptor units to give high triplet energy. In addition, the physical property of the host can be systematically modulated through the different ratios of the electron- and hole-transporting components. Compared to mCP-BPBI, CP-QPBI, with extended benzimidazole moieties, not only improves the thermal stability and film forming ability for effectively solution process but also enhances the electron-transport ability in amorphous thin film by reducing the reorganization energy, which will facilitate the charge balance in the EML. Meanwhile, the increased electron-withdrawing unit deepens the LUMO of CP-QPBI, which indicates the electron-injection barrier to EML should be decreased in the devices. Therefore, selectively enhancing the electron injection and transporting properties without changing the triplet energy was successfully realized. The advantages of the multielectron transporting systems were further demonstrated by their FIrpic- and $Ir(mppy)_3$-based blue and green PHOLEDs. The operating voltage of solution-processed devices using more electron-transport units CP-QPBI as host was dramatically reduced by ∼3 V compare with the similar devices of mCP-BPBI. Sequentially, the power efficiencies were also improved by 2−2.5 times at the corresponding voltage. Importantly, both the blue and green devices maintain their high efficiency up to the brightness of 1000 cd m^{-2}, which strongly demonstrates that turning the ratio of hole- and electron-transport units of the host for more balanced charge transfer is a promising strategy to achieve high-performance solution-processed device at high brightness. Given the ultralow operating voltage and the high-efficiency and low-efficiency roll-off, our research puts forward a new guideline for the molecular design of amorphous bipolar host materials used in solution-processed PHOLEDs.

AUTHOR INFORMATION

Corresponding Authors

*E-mail: jiangw@seu.edu.cn. (W.J.)
*E-mail: sun@seu.edu.cn. (Y.-M.S.)
*E-mail: duanl@mail.tsinghua.edu.cn. (L.D.)

Notes

The authors declare no competing financial interest.

ACKNOWLEDGMENTS

We are grateful for the grants from the National Natural Science Foundation of China (51103023 and 21173042), National Basic Research Program China (2013CB932902). We are also thankful for the support of the Scientific Research Foundation of Graduate School of Southeast University.

REFERENCES

(1) Yook, K. S.; Lee, J. Y. Small Molecule Host Materials for Solution Processed Phosphorescent Organic Light-Emitting Diodes. *Adv. Mater.* **2014**, *26*, 4218−4233.

(2) Zhao, Y.; Duan, L.; Zhang, D. Q.; Hou, L. D.; Qiao, J.; Wang, L. D.; Qiu, Y. Small Molecular Phosphorescent Organic Light-Emitting Diodes Using a Spin-Coated Hole Blocking Layer. *Appl. Phys. Lett.* **2012**, *100*, 083304−083303.

(3) Burroughes, J. H.; Bradley, D. D. C.; Brown, A. R.; Marks, R. N.; Mackay, K.; Friend, R. H.; Burns, P. L.; Holmes, A. B. Light-Emitting-Diodes Based on Conjugated Polymers. *Nature* **1990**, *347*, 539−541.

DOI: 10.1021/acsami.5b00510
ACS Appl. Mater. Interfaces 2015, 7, 7303−7314

(4) Duan, L.; Hou, L. D.; Lee, T. W.; Qiao, J.; Zhang, D. Q.; Dong, G. F.; Wang, L. D.; Qiu, Y. Solution Processable Small Molecules for Organic Light-Emitting Diodes. *J. Mater. Chem.* **2010**, *20*, 6392−6407.
(5) Liu, C.; Li, Y. H.; Li, Y. F.; Yang, C. L.; Wu, H. B.; Qin, J. G.; Cao, Y. Efficient Solution-Processed Deep-Blue Organic Light-Emitting Diodes Based on Multibranched Oligofluorenes with a Phosphine Oxide Center. *Chem. Mater.* **2013**, *25*, 3320−3327.
(6) Gather, M. C.; Kohnen, A.; Falcou, A.; Becker, H.; Meerholz, K. Solution-Processed Full-Color Polymer Organic Light-Emitting Diode Displays Fabricated by Direct Photolithography. *Adv. Funct. Mater.* **2007**, *17*, 191−200.
(7) Ge, Z.; Hayakawa, T.; Ando, S.; Ueda, M.; Akiike, T.; Miyarnoto, H.; Kajita, T.; Kakimoto, M. A. Solution-Processible Bipolar Triphenylamine-Benzimidazole Derivatives for Highly Efficient Single-Layer Organic Light-Emitting Diodes. *Chem. Mater.* **2008**, *20*, 2532−2537.
(8) Xu, H.; Yu, D. H.; Liu, L. L.; Yan, P. F.; Jia, L. W.; Li, G. M.; Yue, Z. Y. Small Molecular Glasses Based on Multiposition Encapsulated Phenyl Benzimidazole Iridium(III) Complexes: Toward Efficient Solution-Processable Host-Free Electrophosphorescent Diodes. *J. Phys. Chem. B* **2010**, *114*, 141−150.
(9) Feng, S.; Duan, L.; Hou, L. D.; Qiao, J.; Zhang, D. Q.; Dong, G. F.; Wang, L. D.; Qiu, Y. A Comparison Study of the Organic Small Molecular Thin Films Prepared by Solution Process and Vacuum Deposition: Roughness, Hydrophilicity, Absorption, Photoluminescence, Density, Mobility, and Electroluminescence. *J. Phys. Chem. C* **2011**, *115*, 14278−14284.
(10) Wu, H.; Ying, L.; Yang, W.; Cao, Y. Progress and Perspective of Polymer White Light-Emitting Devices and Materials. *Chem. Soc. Rev.* **2009**, *38*, 3391.
(11) Adachi, C.; Baldo, M. A.; Thompson, M. E.; Forrest, S. R. Nearly 100% Internal Phosphorescence Efficiency in an Organic Light-Emitting Device. *J. Appl. Phys.* **2001**, *90*, 5048−5051.
(12) Baldo, M. A.; O'Brien, D. F.; You, Y.; Shoustikov, A.; Sibley, S.; Thompson, M. E.; Forrest, S. R. Highly Efficient Phosphorescent Emission from Organic Electroluminescent Devices. *Nature* **1998**, *395*, 151−154.
(13) Sasabe, H.; Nakanishi, H.; Watanabe, Y.; Yano, S.; Hirasawa, M.; Pu, Y. J.; Kido, J. Extremely Low Operating Voltage Green Phosphorescent Organic Light-Emitting Devices. *Adv. Funct. Mater.* **2013**, *23*, 5550−5055.
(14) Liaptsis, G.; Meerholz, K. Crosslinkable TAPC-Based Hole-Transport Materials for Solution-Processed Organic Light-Emitting Diodes with Reduced Efficiency Roll-Off. *Adv. Funct. Mater.* **2013**, *23*, 359−365.
(15) Liaptsis, G.; Hertel, D.; Meerholz, K. Solution Processed Organic Double Light-Emitting Layer Diode Based on Cross-Linkable Small Molecular Systems. *Angew. Chem., Int. Ed.* **2013**, *52*, 9563−9567.
(16) Aizawa, N.; Pu, Y. J.; Sasabe, H.; Kido, J. Thermally Cross-Linkable Host Materials for Enabling Solution-Processed Multilayer Stacks in Organic Light-Emitting Devices. *Org. Electron.* **2013**, *14*, 1614−1620.
(17) Jiang, W.; Xu, H. G.; Ban, X. X.; Yuan, G. L.; Sun, Y. M.; Huang, B.; Duan, L.; Qiu, Y. Alcohol-Soluble Electron-Transport Small Molecule for Fully Solution-Processed Multilayer White Electrophosphorescent Devices. *Org. Lett.* **2014**, *16*, 1140−1143.
(18) Small, C. E.; Tsang, S. W.; Kido, J.; So, S. K.; So, F. Origin of Enhanced Hole Injection in Inverted Organic Devices with Electron Accepting Interlayer. *Adv. Funct. Mater.* **2012**, *22*, 3261−3266.
(19) Pu, Y. J.; Chiba, T.; Aizawa, N.; Sasabe, H.; Kido, J. Multilayered Organic Light-Emitting Devices by Solution-Process. *J. Photopolym. Sci. Technol.* **2013**, *26*, 403−410.
(20) Chaskar, A.; Chen, H. F.; Wong, K. T. Bipolar Host Materials: a Chemical Approach for Highly Efficient Electrophosphorescent Devices. *Adv. Mater.* **2011**, *23*, 3876−3895.
(21) Sasabe, H.; Kido, J. Development of High Performance OLEDs for General Lighting. *J. Mater. Chem. C* **2013**, *1*, 1699−1707.
(22) Su, S. J.; Cai, C.; Kido, J. RGB Phosphorescent Organic Light-Emitting Diodes by Using Host Materials with Heterocyclic Cores: Effect of Nitrogen Atom Orientations. *Chem. Mater.* **2011**, *23*, 274−284.
(23) Sasabe, H.; Toyota, N.; Nakanishi, H.; Ishizaka, T.; Pu, Y. J.; Kido, J. 3,3′-Bicarbazole-Based Host Materials for High-Efficiency Blue Phosphorescent OLEDs with Extremely Low Driving Voltage. *Adv. Mater.* **2012**, *24*, 3212−3217.
(24) Sasabe, H.; Seino, Y.; Kimura, M.; Kido, J. A m-Terphenyl-Modifed Sulfone Derivative as a Host Material for High-Efficiency Blue and Green Phosphorescent OLEDs. *Chem. Mater.* **2012**, *24*, 1404−1406.
(25) Debeaux, M.; Thesen, M. W.; Schneidenbach, D.; Hopf, H.; Janietz, S.; Kruger, H.; Wedel, A.; Kowalsky, W.; Johannes, H. H. Charge-Transporting Polymers based on Phenylbenzoimidazole Moieties. *Adv. Funct. Mater.* **2010**, *20*, 399−408.
(26) Jankus, V.; Monkman, A. P. Is Poly(vinylcarbazole) a Good Host for Blue Phosphorescent Dopants in PLEDs? Dimer Formation and Their Effects on the Triplet Energy Level of Poly(N-vinylcarbazole) and Poly(N-Ethyl-2-Vinylcarbazole). *Adv. Funct. Mater.* **2011**, *21*, 3350−3356.
(27) Yang, X.; Müller, D. C.; Neher, D.; Meerholz, K. Highly Efficient Polymeric Electrophosphorescent Diodes. *Adv. Mater.* **2006**, *18*, 948−954.
(28) Han, C.; Zhang, Z.; Xu, H.; Yue, S.; Li, J.; Yan, P.; Deng, Z.; Zhao, Y.; Yan, P.; Liu, S. Short-Axis Substitution Approach Selectively Optimizes Electrical Properties of Dibenzothiophene-Based Phosphine Oxide Hosts. *J. Am. Chem. Soc.* **2012**, *134*, 19179−19188.
(29) Wu, H. B.; Zou, J. H.; Liu, F.; Wang, L.; Mikhailovsky, A.; Bazan, G. C.; Yang, W.; Cao, Y. Efficient Single Active Layer Electrophosphorescent White Polymer Light-Emitting Diodes. *Adv. Mater.* **2008**, *20*, 696−702.
(30) Ding, J. Q.; Zhang, B. H.; Lu, J. H.; Xie, Z. Y.; Wang, L. X.; Jing, X. B.; Wang, F. S. Solution-Processable Carbazole-Based Conjugated Dendritic Hosts for Power-Efficient Blue-Electrophosphorescent Devices. *Adv. Mater.* **2009**, *21*, 4983−4986.
(31) Zhang, B.; Tan, G.; Lam, C. S.; Yao, B.; Ho, C. L.; Liu, L.; Xie, Z.; Wong, W. Y.; Ding, J.; Wang, L. High-Efficiency Single Emissive Layer White Organic Light-Emitting Diodes Based on Solution-Processed Dendritic Host and New Orange-Emitting Iridium Complex. *Adv. Mater.* **2012**, *24*, 1873−1877.
(32) Li, J. Y.; Zhang, T.; Liang, Y. J.; Yang, R. X. Solution-Processible Carbazole Dendrimers as Host Materials for Highly Efficient Phosphorescent Organic Light-Emitting Diodes. *Adv. Funct. Mater.* **2013**, *23*, 619−628.
(33) Jiang, W.; Ge, Z. J.; Cai, P. Y.; Huang, B.; Dai, Y. Q.; Sun, Y. M.; Qiao, J.; Wang, L. D.; Duan, L.; Qiu, Y. Star-Shaped Dendritic Hosts Based on Carbazole Moieties for Highly Efficient Blue Phosphorescent OLEDs. *J. Mater. Chem.* **2012**, *22*, 12016−12022.
(34) Jiang, W.; Tang, J. N.; Yang, W.; Ban, X. X.; Huang, B.; Dai, Y. Q.; Sun, Y. M.; Duan, L.; Qiao, J.; Wang, L. D.; Qiu, Y. Synthesis of Carbazole-Based Dendrimer: Host Material for Highly Efficient Solution-Processed Blue Organic Electrophosphorescent Diodes. *Tetrahedron* **2012**, *68*, 5800−5805.
(35) Sasabe, H.; Tanaka, D.; Yokoyama, D.; Chiba, T.; Pu, Y.-J.; Nakayama, K.-i.; Yokoyama, M.; Kido, J. Influence of Substituted Pyridine Rings on Physical Properties and Electron Mobilities of 2-Methylpyrimidine Skeleton-Based Electron Transporters. *Adv. Funct. Mater.* **2011**, *21*, 336−342.
(36) Liu, M.; Su, S. J.; Jung, M. C.; Qi, Y. B.; Zhao, W. M.; Kido, J. Hybrid Heterocycle-Containing Electron-Transport Materials Synthesized by Regioselective Suzuki Cross-Coupling Reactions for Highly Efficient Phosphorescent OLEDs with Unprecedented Low Operating Voltage. *Chem. Mater.* **2012**, *24*, 3817−3827.
(37) Zhao, J.; Xie, G.-H.; Yin, C.-R.; Xie, L.-H.; Han, C.-M.; Chen, R.-F.; Xu, H.; Yi, M.-D.; Deng, Z.-P.; Chen, S.-F.; Zhao, Y.; Liu, S.-Y.; Huang, W. Harmonizing Triplet Level and Ambipolar Characteristics of Wide-Gap Phosphine Oxide Hosts toward Highly Efficient and Low Driving Voltage Blue and Green PHOLEDs: An Effective Strategy Based on Spiro-Systems. *Chem. Mater.* **2011**, *23*, 5331−5339.

DOI: 10.1021/acsami.5b00510
ACS Appl. Mater. Interfaces 2015, 7, 7303−7314

(38) Ye, J.; Chen, Z.; Fung, M. K.; Zheng, C. J.; Ou, X. M.; Zhang, X. H.; Yuan, Y.; Lee, C. S. Carbazole/Sulfone Hybrid D-pi-A-Structured Bipolar Fluorophores for High-Efficiency Blue-Violet Electroluminescence. *Chem. Mater.* **2013**, *25*, 2630−2637.
(39) Hsu, F. M.; Chien, C. H.; Shih, P. I.; Shu, C. F. Phosphine-Oxide-Containing Bipolar Host Material for Blue Electrophosphorescent Devices. *Chem. Mater.* **2009**, *21*, 1017−1022.
(40) Li, H.; Duan, L.; Zhang, D.; Qiu, Y. Influence of Molecular Packing on Intramolecular Reorganization Energy: A Case Study of Small Molecules. *J. Phys. Chem. C* **2014**, *118*, 14848−14852.
(41) Yamada, T.; Suzuki, F.; Goto, A.; Sato, T.; Tanaka, K.; Kaji, H. Revealing bipolar charge-transport property of 4,4′-N,N′-dicarbazolylbiphenyl (CBP) by quantum chemical calculations. *Org. Electron.* **2011**, *12*, 169−178.
(42) Lee, C.; Waterland, R.; Sohlberg, K. Prediction of Charge Mobility in Amorphous Organic Materials through the Application of Hopping Theory. *J. Chem. Theory Comput.* **2011**, *7*, 2556−2567.
(43) Duan, L.; Qiao, J.; Sun, Y.; Qiu, Y. Strategies to Design Bipolar Small Molecules for OLEDs: Donor-Acceptor Structure and Non-Donor-Acceptor Structure. *Adv. Mater.* **2011**, *23*, 1137−1144.
(44) Ma, C.; Liang, W.; Jiang, D.; Hong, Z.; Qing, L.; Yan, Y. Theoretical Study of the Photophysical and Charge Transport Properties of Novel Fluorescent Fluorine−Boron Compounds. *Mol. Phys.* **2010**, *108*, 667−674.
(45) Pan, J.-H.; Chou, Y.-M.; Chiu, H.-L.; Wang, B.-C. Theoretical Investigations of the Molecular Conformation and Reorganization Energies in the Organic Diamines as Hole-Transporting Materials. *J. Phys. Org. Chem.* **2007**, *20*, 743−753.
(46) Wang, L.; Wu, Y.; Shan, G.-G.; Geng, Y.; Zhang, J.-Z.; Wang, D.-M.; Yang, G.-C.; Su, Z.-M. The Influence of the Diphenylphosphoryl Moiety on the Phosphorescent Properties of Heteroleptic Iridium(iii) Complexes and the OLED Performance: A Theoretical Study. *J. Mater. Chem. C* **2014**, *2*, 2859−2868.
(47) Tse, S. C.; So, S. K.; Yeung, M. Y.; Lo, C. F.; Wen, S. W.; Chen, C. H. The Role of Charge-Transfer Integral in Determining and Engineering the Carrier Mobilities of 9,10-Di(2-naphthyl)anthracene Compounds. *Chem. Phys. Lett.* **2006**, *422*, 354−357.
(48) Ge, Z. Y.; Hayakawa, T.; Ando, S.; Ueda, M.; Akiike, T.; Miyamoto, H.; Kajita, T.; Kakimoto, M. A. Spin-Coated Highly Efficient Phosphorescent Organic Light-Emitting Diodes Based on Bipolar Triphenylamine-Benzimidazole Derivatives. *Adv. Funct. Mater.* **2008**, *18*, 584−590.
(49) Lee, J.; Han, H.; Lee, J.; Yoon, S. C.; Lee, C. Utilization of ″Thiol-ene″ Photo Cross-Linkable Hole-Transporting Polymers for Solution-Processed Multilayer Organic Light-Emitting Diodes. *J. Mater. Chem. C* **2014**, *2*, 1474−1481.
(50) Park, J.; Park, T.; Jeon, W.; Pode, R.; Jang, J.; Kwon, J.; Yu, E.; Chae, M. Small Molecule Interlayer for Solution Processed Phosphorescent Organic Light Emitting Device. *Org. Electron.* **2009**, *10*, 189−193.
(51) Zuniga, C. A.; Abdallah, J.; Haske, W.; Zhang, Y. D.; Coropceanu, I.; Barlow, S.; Kippelen, B.; Marder, S. R. Crosslinking Using Rapid Thermal Processing for the Fabrication of Efficient Solution-Processed Phosphorescent Organic Light-Emitting Diodes. *Adv. Mater.* **2013**, *25*, 1739−1744.
(52) Liaptsis, G.; Hertel, D.; Meerholz, K. Solution Processed Organic Double Light-Emitting Layer Diode Based on Cross-Linkable Small Molecular Systems. *Angew. Chem., Int. Ed.* **2013**, *52*, 9563−9567.

DOI: 10.1021/acsami.5b00510
ACS Appl. Mater. Interfaces 2015, 7, 7303−7314